Proc. Indian Acad. Sci. (Earth Planet. Sci.), Vol. 94, No. 2, July 1985, pp. 159–184.

Short range prediction with a multi-level primitive equation model

S S SINGH
Indian Institute of Tropical Meteorology, Pune 411 005, India

MS received 13 January 1984; revised 6 November 1984

Abstract. A five-level primitive equation model in a (x, y, p, t) coordinate system has been developed. A fairly sophisticated scheme of physical processes has been incorporated in the model. The model physics include air-sea interaction, cumulus parametrization, large scale condensation, dry convective adjustment, horizontal and vertical diffusion and simulated radiation. The initial balance between mass and motion fields has been obtained through a dynamic initialization scheme. The model has been integrated upto 48 hr using input data of a case of monsoon depression. The results of initialization and forecast have been presented and discussed. Wind, temperature and vertical velocity fields have been found to retain the observed map features; after the initialization, however, the surface pressure has been considerably modified. The model produced a reasonably good forecast up to 24 hr as far as the flow fields, rainfall region, structure of the depression and the movement of cyclonic circulation were concerned and beyond that damped rapidly. The rainfall rates were underestimated. Some of the shortcomings of the model are also discussed.

Keywords. Primitive equation model; numerical prediction; monsoon depression.

1. Introduction

A high resolution global model incorporating necessary physical processes is ideally suited for prediction over the monsoon belt. However, for the reason of economy and for the understanding and prediction of regional scale atmospheric systems, a regional model is highly desirable. A few tropical regional models have been developed for the research and experimental forecast and applied to case studies of the Indian summer monsoon (Krishnamurti *et al* 1976; Singh and Saha 1976; Das and Bedi 1978; Bedi *et al* 1976; Singh 1983). This study presents an application of a limited area five-level primitive equation model for prediction over the monsoon region.

2. Model equations

The model equation in a (x, y, p, t) coordinate system on Mercator projection in flux form may be written as

$$\frac{\partial u}{\partial t}+m^2\left[\frac{\partial}{\partial x}\left(u\frac{u}{m}\right)+\frac{\partial}{\partial y}\left(u\frac{v}{m}\right)\right]+\frac{\partial}{\partial p}(\omega u)-f^*v+mg\frac{\partial z}{\partial x}$$

$$=-g\left(\frac{\partial \tau}{\partial p}\right)_x+F_u, \quad (1)$$

$$\frac{\partial v}{\partial t}+m^2\left[\frac{\partial}{\partial x}\left(v\frac{u}{m}\right)+\frac{\partial}{\partial y}\left(v\frac{v}{m}\right)\right]+\frac{\partial}{\partial p}(\omega v)+f^*u+mg\frac{\partial z}{\partial y}$$
$$=-g\left(\frac{\partial \tau}{\partial p}\right)_y+F_v, \quad (2)$$

$$\partial z/\partial p=-RT_v/pg, \quad (3)$$

$$m^2\left[\frac{\partial}{\partial x}\left(\frac{u}{m}\right)+\frac{\partial}{\partial y}\left(\frac{v}{m}\right)\right]+\frac{\partial \omega}{\partial p}=0, \quad (4)$$

$$\frac{\partial p_s}{\partial t}+mu_s\frac{\partial p_s}{\partial x}+mv_s\frac{\partial p_s}{\partial y}-\omega_s=0, \quad (5)$$

$$\frac{\partial}{\partial t}(C_pT)+m^2\left[\frac{\partial}{\partial x}\left(C_pT\frac{u}{m}\right)+\frac{\partial}{\partial y}\left(C_pT\frac{v}{m}\right)\right]+g\frac{\partial z}{\partial p}\omega$$
$$=\frac{dQ}{dt}-g\frac{\partial H}{\partial p}+C_pF_T, \quad (6)$$

$$\frac{\partial q}{\partial t}+m^2\left[\frac{\partial}{\partial x}\left(q\frac{u}{m}\right)+\frac{\partial}{\partial y}\left(q\frac{v}{m}\right)\right]+\frac{\partial}{\partial p}(q\omega)=M-g\frac{\partial W}{\partial p}+F_q, \quad (7)$$

$$T_v=T(1+0{\cdot}62q) \quad (8)$$

Equations (1) and (2) are the equations of motion in the east and north directions respectively. Equation (3) represents the hydrostatic law and (4) is the continuity equation. Equations (5) and (6) represent the surface pressure tendency and thermodynamic energy equation respectively. Equation (7) represents the moisture continuity equation and (8) is the virtual temperature correction equation.

3. Model structure and data

The domain of integration extends from 6°N to 36°N and 56°E to 106°E. The area is resolved by the uniform grid interval of 220 km on the Mercator projection. In the horizontal all the variables are defined at the same grid point (non-staggered grid). In the vertical, the model has four layers between 100 mb and 900 mb, with a spacing of 200 mb and a fifth layer of approximately 100 mb thickness between 900 mb and the ground surface (figure 1). The horizontal wind components and the geopotential height are specified at levels 200, 400, 600, 800 and 950 mb and the temperature, the specific humidity and the vertical velocity are set at 300, 500, 700 and 900 mb. Vertical velocity is assumed zero at 100 mb and computed at the lower boundary through continuity equation. The temperature field between 950 mb and the ground surface is extrapolated at each time-step from those of 700 and 900 mb. In the boundary layer between 950 mb and ground surface, no wind shear is assumed. The input data of 4 and 5 August 1968 have been chosen for the prediction experiment. Both days refer to the mature stage of a monsoon depression. Wind and temperature data are available at all standard pressure levels upto 100 mb, however there is no moisture observation beyond 500 mb level. Since the specific humidity (q) is required at 300 mb also, this is computed using the relative humidity value of 500 mb and the temperature of 300 mb.

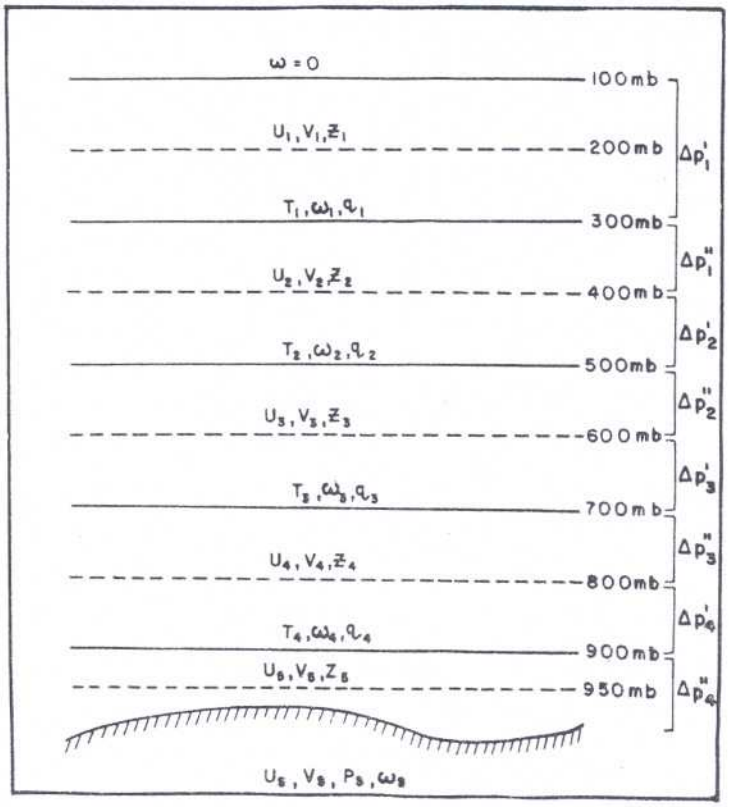

Figure 1. Vertical structure of five level primitive equation model.

In other words, no vertical variation in relative humidity beyond 500 mb level is assumed. A time step of 5 min for the grid length chosen was found suitable.

4. Boundary conditions

Rigid walls are specified between two outermost rows of gridpoints in the north and south directions where the normal component of motion vanishes, but tangential flow is permitted. In the east-west direction cyclic continuity is adopted by extending the domain by eight additional grid points on the eastern side and the variables are specified as

$$Q(L+8) = Q(2) \quad \text{and} \quad Q(1) = Q(L+7),$$

where L is the number of grid points in the east-west direction in the unextended domain and Q stands for any variable such as u, v, etc. Data in the extended domain are obtained by fitting a cubic polynomial using values of grid points $L-1$, L, $L+7$ and $L+8$. The lateral boundary conditions are used to determine u, v, T, q, and P_s at the

outermost grid points using values of grid point inside. Following the above procedure the variables may be specified as follows at the north-south boundary,

$$\frac{\partial u}{\partial y} = \frac{\partial T}{\partial y} = \frac{\partial q}{\partial y} = \frac{\partial p_s}{\partial y} = 0; \quad \bar{v}^y = 0,$$

where $\bar{v}^y$ denotes the mean northward wind speed over the two outermost rows. For the evaluation of pressure tendency, u_s and v_s must be known. This is done by assuming zero wind shear between 950 mb and the ground surface. Using the above criterion, wind at the lower boundary may be specified,

$$u_s = u_{950}: \quad v_s = v_{950}.$$

5. Finite difference scheme

Following Okamura (1975), mass and energy conserving finite difference scheme for space derivatives has been adopted. We define the following two basic operators for finite differencing. The first operator is a finite difference form for the divergence of two physical quantities A and B,

$$D_x(A * B)_i \equiv \frac{1}{8d\Delta p_i}\big[\{A_{i+1}(\Delta p_{i+1} + \Delta p_i) + A_i(3\Delta p_i - \Delta p_{i-1})\}$$

$$(B_{i+1} + B_i) - \{A_{i-1}(\Delta p_{i-1} + \Delta p_i) + A_i(3\Delta p_i - \Delta p_{i-1})\}(B_i + B_{i-1})\big], \qquad (9)$$

where i denotes the grid point in the x-direction, Δp_i the thickness of a layer in pressure difference, d the grid interval, D_x the finite difference with respect of x. It should be noted that the product $(A * B)$ is asymmetric on the right hand side of (9). A similar operator may be defined for D_y.

The second operator is expressed as

$$G_x(A, B) \equiv \frac{1}{4d}\{(A_{i+1} + A_i)(B_{i+1} - B_i) + (A_i + A_{i-1})(B_i - B_{i-1})\} \qquad (10)$$

This is the finite difference scheme for the product of A and the derivative of B with respect to x. A similar operator may be defined for G_y. The centred difference scheme using three data levels has been adopted for vertical derivatives.

These operators ensure the energy conservation property of the governing equations in the finite difference form. Applying (9) and (10) to (1) through (8), the finite difference equations of the model equations are obtained. For marching in time, the Leapfrog scheme with an Asselin (1972) time filter is adopted.

6. Physical processes

6.1 *Sub-grid scale horizontal diffusion*

Horizontal diffusion is introduced in the momentum, thermodynamic and water vapour equations. A simple linear diffusion formula is used in the model as,

$$F_\alpha = \nu\nabla^2\alpha, \quad \alpha = u, v, T \text{ or } q.$$

The value of coefficient ν is determined following Leith (1969),

$$\nu = \gamma |\nabla \zeta| d^3$$

where ζ is relative vorticity, d the grid distance, and γ is the empirically determined non-dimensional constant being set to 0·25.

6.2 Surface friction

The exchange of momentum between the air and the earth's surface in the surface layer is expressed by the stress vector

$$\tau = \rho C_D' |\mathbf{V}_m| \mathbf{V}_m,$$

where $C_D' = 0{\cdot}75\, C_D''$ and $\mathbf{V}_m$ is the wind vector at $Z = Z_m (= 10\text{ m})$. The coefficient C_D'' (relation for computing C_D'' is given in §6.3) is calculated over the sea surface. The coefficient over the land is set three times as large as the maximum value of C_D' over the sea surface. The following relation is used for stress at 900 mb and above,

$$\tau_{900} = \rho Km \left(\frac{\partial \mathbf{V}}{\partial Z}\right)_{900} \qquad (p \geqslant 900\text{ mb}),$$

$$\tau = 0 \qquad (p < 900\text{ mb})$$

where $Km = l^2 \left|\left(\frac{\partial \mathbf{V}}{\partial Z}\right)\right|_{900}$ and $l = 30$ m.

6.3 *Surface exchange of sensible heat and moisture*

The exchange of heat and moisture is evaluated by the bulk method and over land is set as zero.

In the bulk method, sensible heat flux from the sea surface, H_0 may be given as

$$H_0 = \rho C_D'' C_p |\mathbf{V}_m| (T_0 - T_a).$$

For an unstable and neutral case:

$$(\Delta T = T_0 - T_a \geqslant 0)$$

$$C_D'' = (1{\cdot}0 + 0{\cdot}066\,\Delta T) \times (0{\cdot}883 + 0{\cdot}084 |\mathbf{V}_m|) \times 10^{-3}.$$

For a stable case:

$$\Delta T = T_0 - T_a < 0$$

$$C_D'' = (1{\cdot}0 + 0{\cdot}111\,\Delta T) \times (0{\cdot}889 + 0{\cdot}055 |\mathbf{V}_m|) \times 10^{-3},$$

where T_0 is sea surface temperature and T_a the temperature of the air at the altitude of Z_m (10 m).

Surface flux of water vapour (evaporation) is evaluated by the same formula as that of sensible heat

$$W_0 = \rho C_D'' |\mathbf{V}_m| [q(T_0) - q(T_a)]$$

where $q(T_0)$ and $q(T_a)$ are specific humidity at sea surface temperature T_0, and at air temperature T_a.

Vertical eddy diffusion of sensible heat and moisture is evaluated in the following way:

$$H_0 = 0, \qquad p < 900 \text{ mb}$$

$$W = -\rho K m \frac{\partial q}{\partial z}, \quad Km = l^2 \left|\frac{\partial \mathbf{V}}{\partial z}\right|, \quad p \geqslant 700 \text{ mb},$$

$$W = 0. \qquad p < 700 \text{ mb}$$

H_0, C_D'' and W_0 are computed following Electronic Computation Centre (1980).

6.4 *Dry convective adjustment*

Dry convective adjustment is performed wherever superadiabatic lapse rates $(-\partial T/\partial p) > \gamma_d)$ were encountered. Following Kanamitsu (1975), the adjustment modifies the vertical temperature distribution while preserving the dry static energy.

6.5 *Large scale condensation and stable heating*

If the relative humidity reaches 100%, large scale condensation is assumed to take place. The relative humidity is not allowed to exceed 100% as the excess water vapour is condensed instantaneously and humidity values are brought to their saturation values. Appropriate heating and humidity changes are introduced in the model equations following Manabe *et al* (1965). The scheme is briefly presented below.

The specific humidity (δq) and temperature (δT) are adjusted by solving the equation,

$$q + \delta q = q_s(T + \delta T, p),$$

$$C_p \delta T + L \delta q = 0.$$

Iterative procedures for solving the above equations are adopted following Manabe *et al* (1965). The condensed rain for the entire column is given by

$$P_r \text{ (large scale)} = -\frac{1}{g}\int_{100}^{p_s} \delta q \, \mathrm{d}p.$$

6.6 *Parametrization of cumulus convection*

The parametrization of cumulus convective scheme of Kuo (1965, 1974) modified by Kanamitsu (1975) and Krishnamurti *et al* (1976) has been invoked for computation of convective transport of heat and moisture. The large scale supply of moisture I is defined by the relation,

$$I = \frac{1}{g}\int_{P_b}^{P_T} \omega \frac{\partial q}{\partial p} \mathrm{d}p,$$

where P_b denotes the cloud base which is here identified with the lifting condensation level (LCL) and P_T denotes the cloud top and is determined from an intersection of the local moist adiabat (through LCL) with the environmental sounding in the upper troposphere.

I is partitioned into

$$I = I_\theta + I_q,$$

or

$$I_q = bI,\ I_\theta = (1-b)I,$$

where I_θ is the part of the moisture supply which goes into enhancing the temperature field and I_q is a part that modifies the moisture field and b is the fraction of available moisture supply that modifies the moisture field. Two other quantities Q_θ and Q_q are determined by the relations

$$Q_\theta = -\frac{C_p}{Lg}\int_{P_B}^{P_T}\left[\left(\frac{T_s - T}{\Delta t}\right) + \frac{T}{\theta}\omega\frac{\partial\theta}{\partial p}\right]\mathrm{d}p,$$

$$Q_q = -\frac{1}{g}\int_{P_B}^{P_T}\left(\frac{q_s - q}{\Delta t}\right)\mathrm{d}p.$$

Here Δt denotes the cloud time scale. These two quantities Q_θ and Q_q are known and $Q = Q_\theta + Q_q$ is a measure of total moisture supply needed to cover a volume over a horizontal area with clouds. The two unknowns a_θ and a_q for (11) and (12) are defined by the relations,

$$a_\theta = I_\theta / Q_\theta,$$

$$a_q = I_q / Q_q.$$

Following Kuo (1965), the convective heating and moisture transport by convection at each level is expressed as follows:

$$\frac{\partial\theta}{\partial t} = -\omega\frac{\partial\theta}{\partial p} + a_\theta\left[\omega\frac{\partial\theta}{\partial p} + \frac{\theta}{T}\left(\frac{T_s - T}{\Delta t}\right)\right], \tag{11}$$

$$\frac{\partial q}{\partial t} = a_q\left(\frac{q_s - q}{\Delta t}\right), \tag{12}$$

and

$$\int\frac{C_p T}{L\theta}\frac{\partial\theta}{\partial t}\mathrm{d}p = A + (1-b)I, \tag{13}$$

$$\int\frac{\partial q}{\partial t}\mathrm{d}p = bI, \tag{14}$$

where

$$A = -\frac{1}{g}\int\frac{C_p}{L}\frac{T}{\theta}\omega\frac{\partial\theta}{\partial p}\mathrm{d}p.$$

In the prediction model, the cumulus scale heating and vertical flux of moisture are invoked only if the sounding is conditionally unstable and the net large scale convergence of flux of moisture in the vertical column is positive. In order to determine

b, (13) and (14) are equated to close the system. Thus,

$$b = (A + I)/2I,$$

$$a_q = (A + I)/2Q_q,$$

$$a_\theta = (I - A)/2Q_\theta.$$

The cloud time scale, Δt is set equal to 30 min in this experiment.

7. Initialization

The simplest initialization procedure for the primitive equation model is to balance mass and motion fields through a nonlinear balance equation. In this method geopotentials are obtained from nondivergent wind through a reverse balance equation and temperature is derived through hydrostatic relation. Vertical motion and horizontal divergence are set to zero initially. Singh and Saha (1976) and Singh (1977) applied this scheme of initialization to predict a case of monsoon depression and of tropical cyclone. Round-the-clock forecast movement of cyclonic circulation and flow patterns were reasonably good; but the temperature lapse rate in the initial and forecast fields were far from satisfactory mainly due to poor boundary conditions for the solution of the balance equation.

Kanamitsu (1975) and Kiangi (1977) showed that the dynamic initialization is superior to static initialization (balance equation solution) for the initial adjustment of mass and motion fields for the tropical atmosphere. The success of dynamic initialization experiment (Singh *et al* 1980) for the barotropic prediction of monsoon depression and the failure to obtain the realistic temperature and vertical velocity fields in an earlier version of the model (Singh and Saha 1976) motivated us to apply the dynamic initialization scheme for the present study. The formulation is essentially the same as that followed by Winninghoff (1973) and Kanamitsu (1975).

For the application of dynamic initialization the variables u, v, T, q, P_s are needed as inputs to the model. The observed wind field is initially modified so that the vertical motion at the lowest level of the model vanishes. This step is necessary to suppress the external gravity waves, at least initially and is called pre-initialization.

7.1 *Pre-initialization*

(i) From the observed wind, the stream function (ψ) and nondivergent part of wind u_ψ and v_ψ at each level are evaluated by the relation

$$\nabla^2\psi = m^2\left[\frac{\partial}{\partial x}\left(\frac{v_{ob}}{m}\right) - \frac{\partial}{\partial y}\left(\frac{u_{ob}}{m}\right)\right],$$

$$u_\psi = -m\frac{\partial\psi}{\partial y}, \quad v_\psi = m\frac{\partial\psi}{\partial x}.$$

(ii) The horizontal divergence from the observed wind at each level is computed. The divergence is adjusted such that the net divergence in a vertical column vanishes. Since the net divergence computed from the observed wind may not vanish, the correction in

the divergence field is applied at levels where observations and analyses are not considered the best. The 200, 800 mb and surface levels are considered the best quality levels due to the large number of surface observations, pibal observations, commercial aircraft reports and satellite cloud motion vectors and as such the correction is applied only at 400 and 600 mb levels; at 200, 800 mb and surface levels the divergence is fixed. This is done through the following relation

$$(\nabla \cdot \mathbf{V})_k^{\text{corrected}} = (\nabla \cdot \mathbf{V})_k^{\text{observed}} - \beta_k \Big/ \left(\sum_{k=1}^{N} \beta_k \Delta p_k \right) \sum_{k=1}^{N} \Delta p_k (\nabla \cdot \mathbf{V})_k^{\text{observed}},$$

where Δp is the pressure difference between the two wind levels, k is the subscript for level and $\beta_k = 1$ for 400 and 600 mb and zero for 200, 800 mb and surface levels.

From the adjusted divergence the irrotational part of wind is evaluated as

$$\nabla^2 \chi = \nabla \cdot \mathbf{V},$$

$$u_\chi = m \frac{\partial \chi}{\partial x}, \quad v_\chi = m \frac{\partial \chi}{\partial y}.$$

(iii) The adjusted wind is computed as

$$u_{\text{adj}} = u_\psi + u_\chi,$$

$$v_{\text{adj}} = v_\psi + v_\chi.$$

The geopotential height (z) is computed from the surface pressure and the observed temperature

$$\partial z / \partial p = -RT_v / pg.$$

Thus, all variables u, v, T, q, z and P_s are known initially.

7.2 *Dynamic initialization*

The common method for obtaining the balanced field through a dynamic initialization scheme is to insert the data for dominant variables into the prognostic equations and integrate back and forth around the initial time, applying a time differencing scheme which tends to suppress the gravity waves but does not affect meteorological component significantly. In the present study, a scheme suggested by Temperton (1976) has been applied. For a typical variable u, one iteration of the scheme is defined by

$$\begin{aligned} u^* &= u^{(\nu)} + \Delta t \left(\frac{\partial u}{\partial t} \right)^{(\nu)}, \\ u^{**} &= u^* - \Delta t \left(\frac{\partial u}{\partial t} \right)^*, \\ u^{\nu+1} &= 3u^{(\nu)} - 2u^{**}, \end{aligned} \tag{15}$$

where ν is the iteration number. It can be shown that in one cycle of iteration a wave of frequency is damped by a factor $1 - 2\Delta t^2 K^2 \sigma^2$. The wave of frequency $K\sigma = \pm 1/(2)^{1/2} \Delta t$ will be completely removed after one cycle, while higher frequency waves will change sign at each iteration.

Although it is desirable to force the mass field to adjust towards wind field, in this experiment no consideration is given to the restoration of any variable and all fields are left free to adjust mutually. The iteration scheme (15) is applied for marching back and forth with Δt positive for odd cycles, which is replaced by $-\Delta t$ for even cycles. The diabatic heating is not incorporated during initialization, although the moisture continuity equation is included for temperature correction. There is very little chance for supersaturation to occur, however if such situation occurs, the excess moisture is removed without effecting any change in the temperature. During the present experiment such a situation did not occur at any grid point.

One step forward as given by (15) and one step backward with $\Delta t = -\Delta t$ constitutes one cycle of iteration. In this experiment ninety such cycles are performed to achieve the initial balance. The number of cycles is chosen arbitrarily as there is no theoretical criterion for achieving the convergence except that root mean square difference for basic fields (u, v, T and P_s) of two successive iterations with an interval of 10 cycles become exceedingly small.

8. Results of initialization experiment

Initialization and forecast results with the input of 4 and 5 August have been found to be similar; hence the results of only one input day i.e. 5 August will be presented and discussed. However, results of 4 August will also be discussed where it is relevant.

Table 1 which presents the root mean square difference for basic fields of two successive iterations, shows that at the end of the initialization experiment the rate of reduction is very slow.

Figures 2, 3, 4 and 5 present fields before and after the initialization of the surface pressure, wind at 800 and 200 mb, temperature at 700 and 300 mb, and vertical velocity at 700 and 300 mb respectively.

It may be seen from figures 2 through 5 that initialization smoothens the patterns of all variables. Maximum changes are noticed in the surface pressure; even the geometry of the circulation system is either lost or completely modified. Kanamitsu (1975) also

Table 1. Root mean square difference between successive iterations (interval of 10 cycles)

Cycle No.	P_s (mb)	u (ms^{-1})					v (ms^{-1})					T (°K)			
		950	800	600	400	200	950	800	600	400	200	900	700	500	300
10	1·44	0·12	0·12	0·12	0·15	0·29	0·16	0·16	0·15	0·18	0·49	0·06	0·08	0·08	0·12
20	0·57	0·08	0·08	0·06	0·06	0·18	0·12	0·11	0·09	0·07	0·31	0·03	0·04	0·05	0·09
30	0·33	0·07	0·07	0·05	0·05	0·14	0·10	0·10	0·08	0·06	0·26	0·02	0·03	0·04	0·08
40	0·23	0·07	0·06	0·05	0·04	0·12	0·10	0·09	0·07	0·05	0·22	0·01	0·03	0·04	0·07
50	0·18	0·06	0·05	0·04	0·04	0·10	0·09	0·08	0·06	0·04	0·19	0·01	0·03	0·03	0·06
60	0·14	0·06	0·05	0·04	0·04	0·09	0·08	0·07	0·06	0·04	0·17	0·01	0·02	0·03	0·05
70	0·12	0·05	0·05	0·03	0·04	0·08	0·07	0·06	0·05	0·04	0·16	0·01	0·02	0·03	0·05
80	0·10	0·05	0·04	0·03	0·03	0·07	0·07	0·06	0·05	0·03	0·14	0·01	0·02	0·03	0·05
90	0·09	0·05	0·04	0·03	0·03	0·06	0·06	0·05	0·04	0·03	0·13	0·01	0·02	0·02	0·04

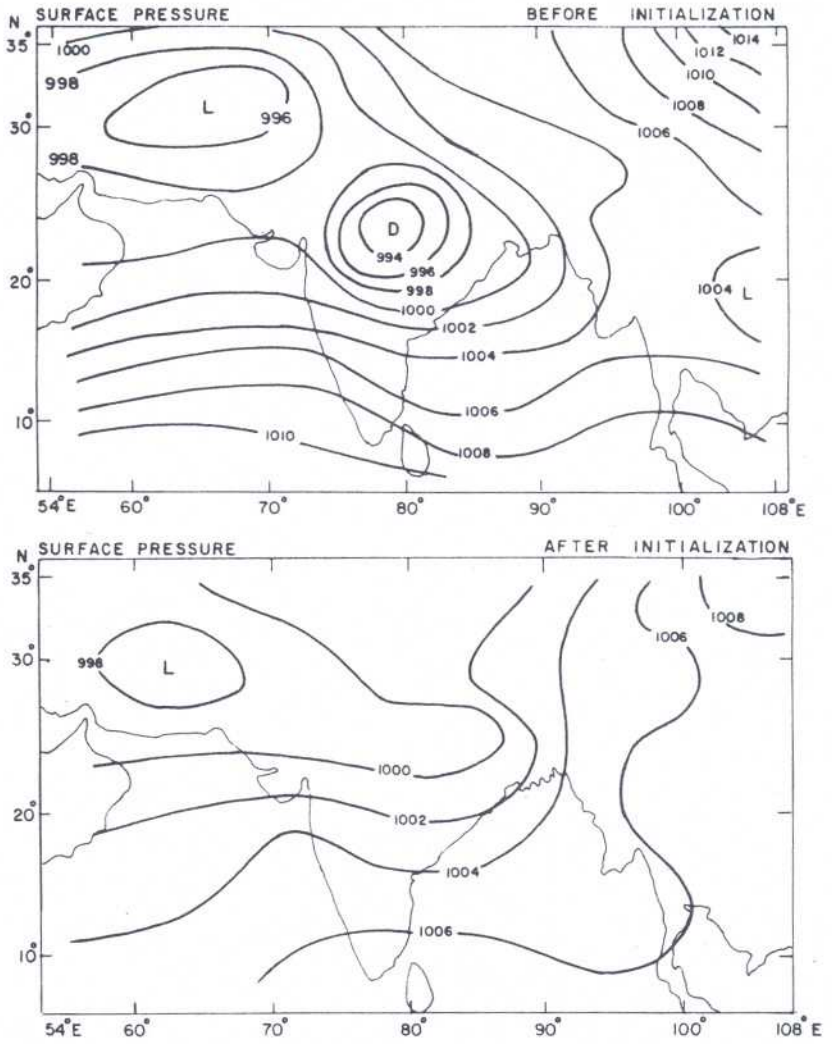

Figure 2. Change of surface pressure by initialization (unit: mb).

found similar results in his dynamic initialization experiment. Adjustment of surface pressure is not only affected by the surface wind but also by the vertically integrated divergence. The change in the surface pressure is obviously the reflection of adjustment of external gravity waves. Figures 3 and 4 and table 2 reveal that other variables like wind and temperature change very little after initialization. The insignificant change in temperature is the reflection of slight adjustment of internal gravity waves.

The vertical velocity patterns (figure 5) are considerably smoothed out without changing the basic patterns. Emergence of large vertical velocity values even after initialisation suggests the importance of the divergent part of the wind in the initial data of the monsoon region particularly for the input to the numerical model.

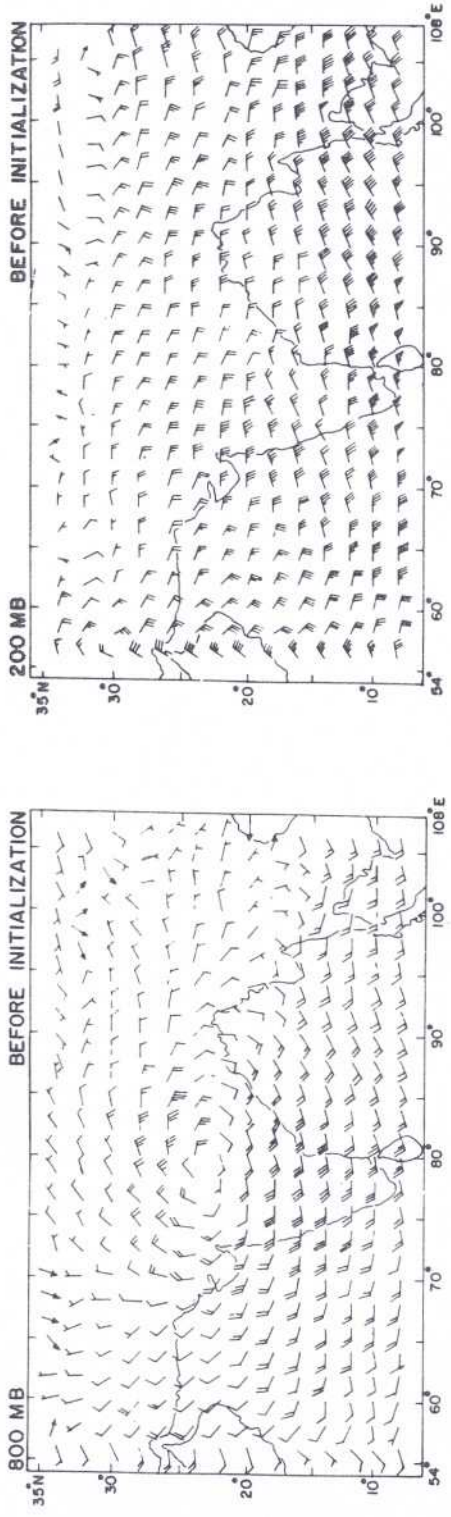

Figure 3a. Change of 800 mb wind by initialization (unit: knot).

Figure 3b. Same as figure 3a except at 200 mb.

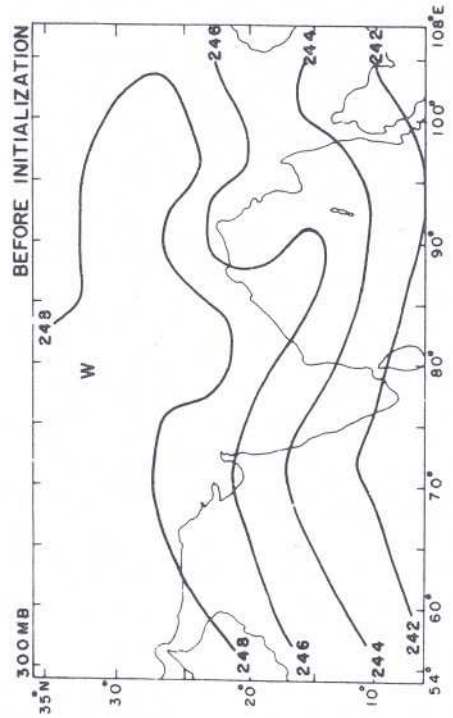

Figure 4b. Same as figure 4a except at 300 mb.

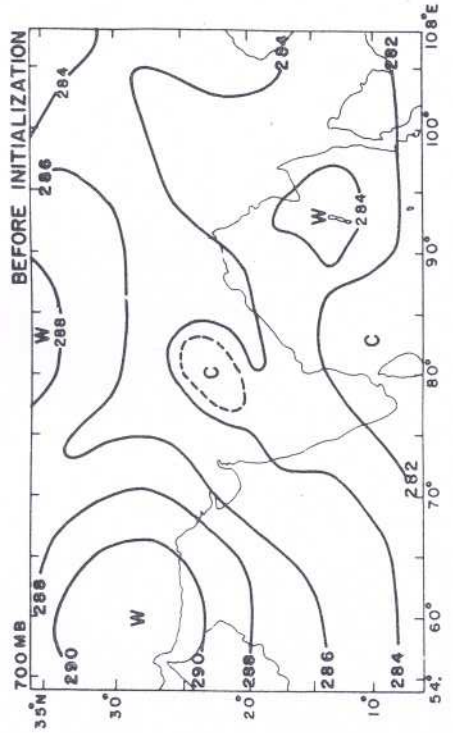

Figure 4a. Change of 700 mb temperature by initialization (unit: K).

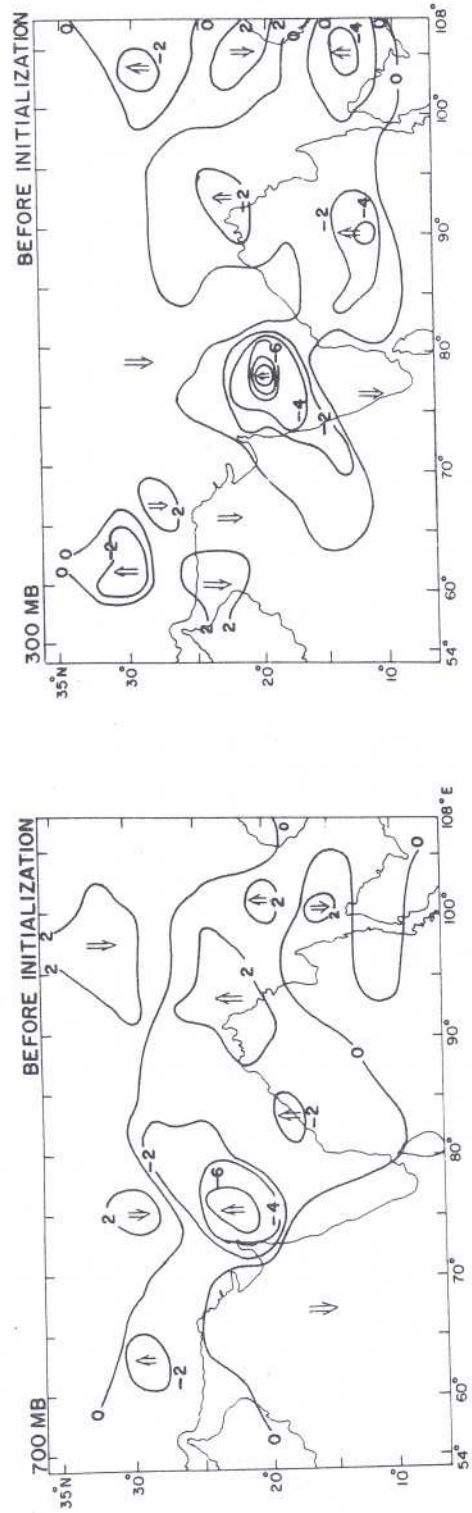

Figure 5a. Change of 700 mb vertical velocity by initialization (unit: 10^{-3} mb sec^{-1}).

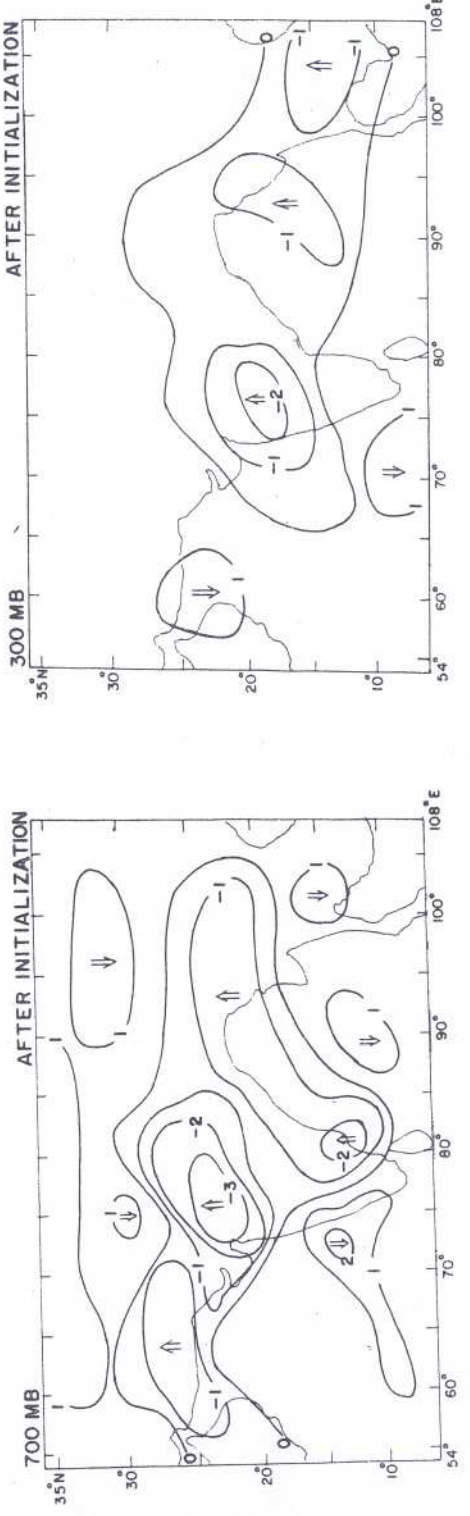

Figure 5b. Same as figure 5a except at 300 mb.

Table 2. Root mean square difference (RMS) between the fields before and after the iterative initialization

Variables	Pressure levels	RMS difference	Variables	Pressure levels	RMS difference
P_s	Surface	2·97 mb	v	400	0·22 ms^{-1}
u	950	0·25 ms^{-1}	u	200	0·52 ms^{-1}
v	950	0·33 ms^{-1}	v	200	0·88 ms^{-1}
u	800	0·23 ms^{-1}	T	900	0·14°K
v	800	0·30 ms^{-1}	T	700	0·22°K
u	600	0·18 ms^{-1}	T	500	0·25°K
v	600	0·25 ms^{-1}	T	300	0·33°K
u	400	0·22 ms^{-1}			

9. Forecast results

The model has been integrated upto 48 hr with the input of 4 and 5 August 1968. As mentioned earlier the results of 5 August only will be presented. As considerable damping is noticed in the 48 hr forecast, the details of the 24 hr forecast are presented and discussed below; wherever necessary, the 48 hr results will also be discussed. Figures 6 and 7 depict the 24 hr forecast and corresponding verification charts in respect of wind at 800 and 200 mb and temperature at 700 and 300 mb respectively. Figure 8 gives the 24 hr forecast and corresponding verification charts in respect of the vertical velocity field at 700 mb. It may be seen from figure 6 that the forecast flow patterns and movement of the cyclonic system have been found reasonably good. The temperature field as seen from figure 7 is very well predicted at 300 mb; however prediction at 700 mb is not good. The upward vertical velocity maximum (figure 8) as expected is found in the western sector of the cyclonic system. The verification vertical velocity is computed from the observed divergence and as such it differs from the forecast vertical velocity. The difference is not merely due to inaccuracy in the forecast but also due to inherent errors in the computation of verification of vertical velocity from the observed divergence.

9.1 *The depression track*

Figure 9 depicts the tracks observed and predicted by one-level and five-level primitive equation models. The 24 hr forecast position of the centre of the depression is slightly better in the five-level primitive equation model; however the movement as seen in 48 hr is slower than the actual; it is also slower than that of barotropic prediction. Generally, the movement of the advecting system is very small as predicted by the barotropic model. Besides, the author has tested the movements of several depressions on the basis of the barotropic model and he finds the movement in the case of this series (4 to 6 August) is best predicted. Furthermore, the slower prediction movement after 24 hr (in the five-level model) may partly be attributed to the complete absence of orography from the model. It is well known that bottom topography can produce faster westward movement of the monsoon depression (Krishnamurti *et al* 1977). The effects of

orography on the westward movement are being investigated and would be reported later.

9.2 *Vertical cross-sections of meridional wind, relative vorticity, temperature anomaly and vertical velocity along a zonal plane passing through 22°N*

9.2a *Meridional wind:* Figure 10 presents the observed and the predicted cross-sections of the meridional wind along a zonal plane passing through 22°N. The predicted northerly and southerly maxima coincide very well with the observed field. Furthermore, the eastward vertical tilt in the lower troposphere and the vertical extent of the cyclonic circulation are very well predicted. The separation distance between northerly and southerly maxima nearly coincide on 5 August; however, this distance is increased in the forecast field on 6 August suggesting broadening of the size of the depression.

9.2b *Relative vorticity:* The observed and the predicted relative vorticity cross-sections are illustrated in figure 11. The vorticity maximum is seen centred over the storm in the lower troposphere as expected. The vorticity maximum and its centre are very well predicted by the model, except that the predicted centre of the maximum lies slightly at a higher level than the observed. In general, the model has produced a good forecast of the vorticity field over the storm.

9.2c *Temperature anomaly:* The observed and the predicted vertical cross-sections of the temperature anomaly (difference from zonal mean) are presented in figure 12. The cold core in the lower troposphere is very well predicted although strong and slightly east of the actual location. The warm core above the storm in the upper troposphere is very well simulated by the model.

9.2d *Vertical velocity:* Figure 13 presents the predicted vertical cross-section of the vertical velocity. It may be seen that the maximum upward motion is centred over the storm in the middle troposphere as expected. Though the model has been successful in the prediction of vertical velocity, intensity has been found slightly weaker than usually expected (3–4 mb S^{-1}) in the intense depression.

9.3 *Rainfall rates*

The 24 hr predicted versus observed rainfall is presented in figure 14. The total rainfall includes the convective and stable precipitation. It may be seen that the most intense rainfall occurs slightly west of the storm centre which has been predicted reasonably well by the model. Furthermore, the region of precipitation is also handled very well by the model. However, the amount in general is very much underestimated (one fifth of the actual). The reasonably good prediction of rainfall rates mainly depend on moisture analyses in the lower troposphere, distribution of vertical velocity, parametrization of cumulus convection and horizontal and vertical resolutions of the model. It is likely that most of the factors outlined above must have contributed to the poor prediction of rainfall rates. We are looking forward to improvement in prediction of rainfall rates in our future experiments.

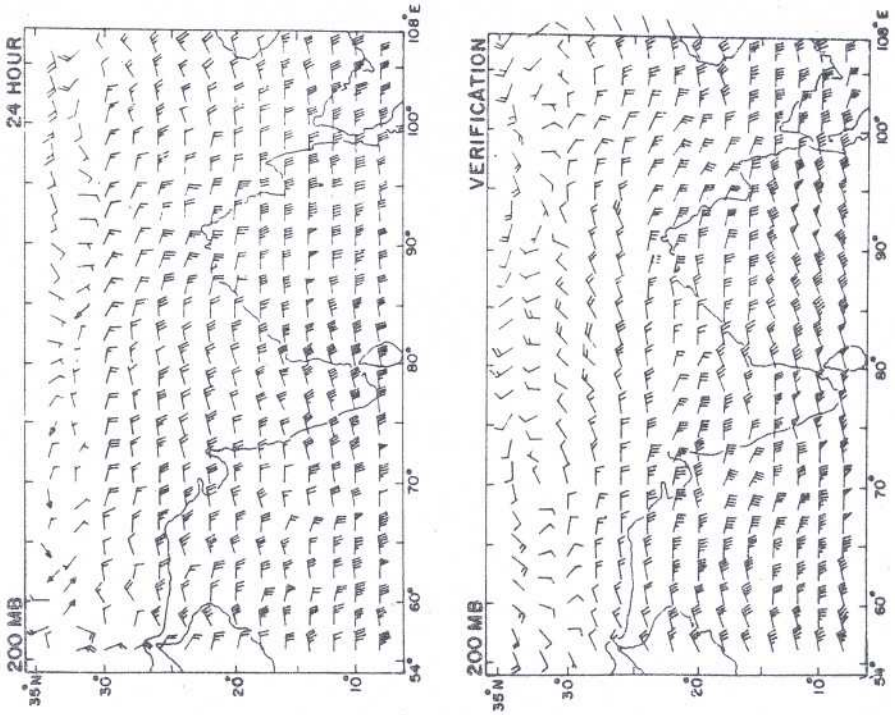

Figure 6b. 24 hr forecast and corresponding verification wind charts at 200 mb (unit: knot).

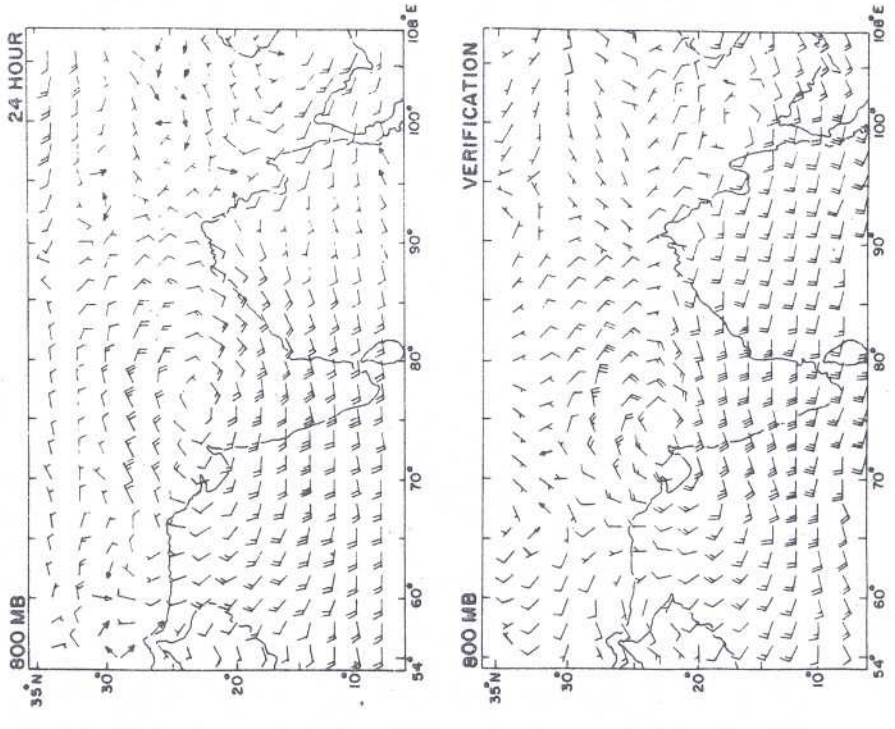

Figure 6a. 24 hr forecast and corresponding verification wind charts at 800 mb (unit: knot).

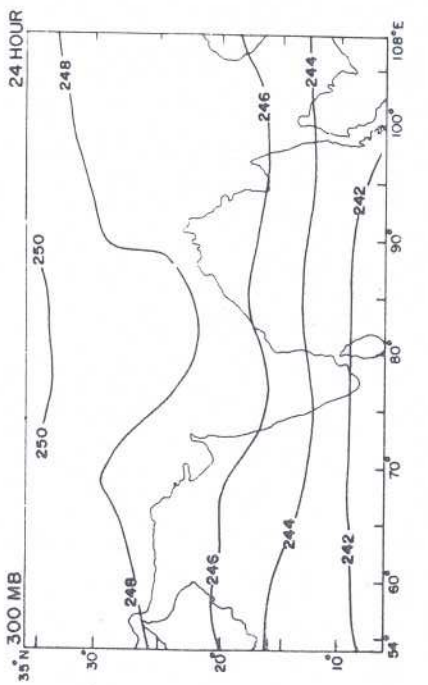

Figure 7b. 24 hr forecast and corresponding verification temperature charts at 300 mb (unit: K).

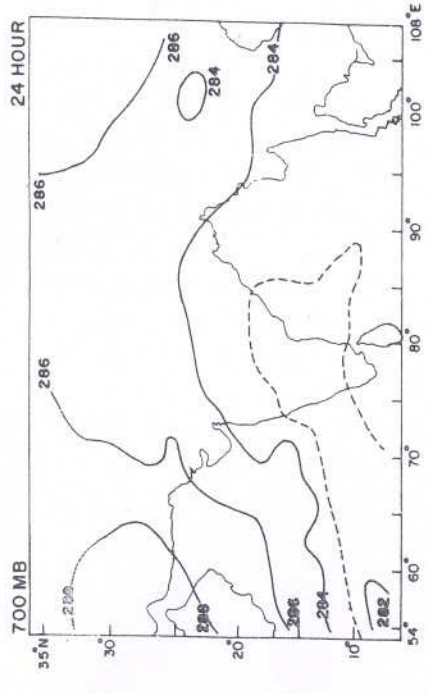

Figure 7a. 24 hr forecast and corresponding verification temperature charts at 700 mb (unit: K).

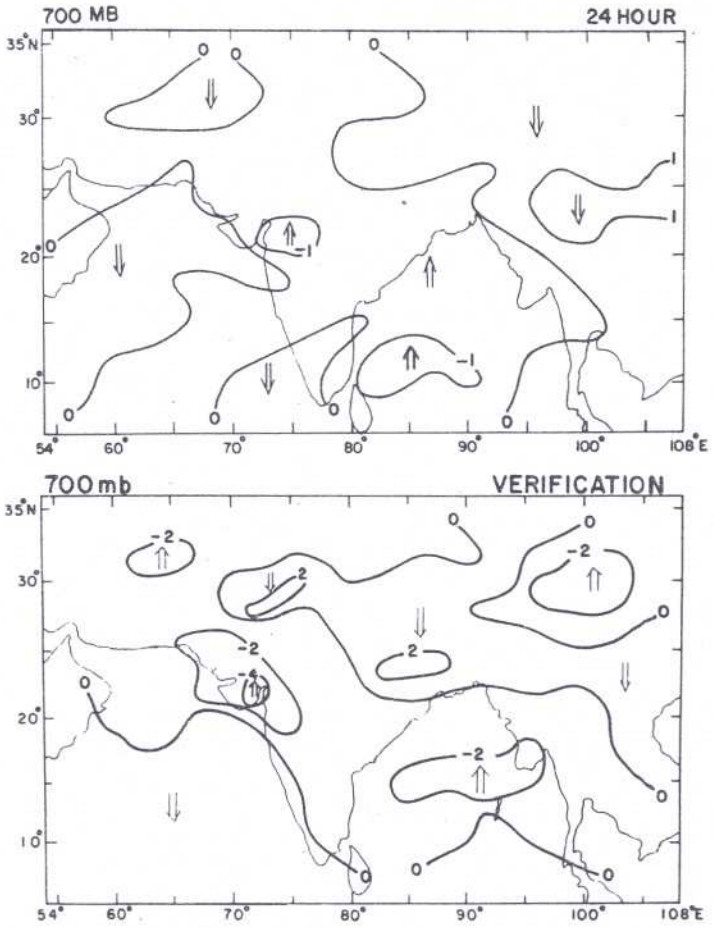

Figure 8. 24 hr forecast and corresponding verification vertical velocity chart at 700 mb (unit: 10^{-3} mb S^{-1}).

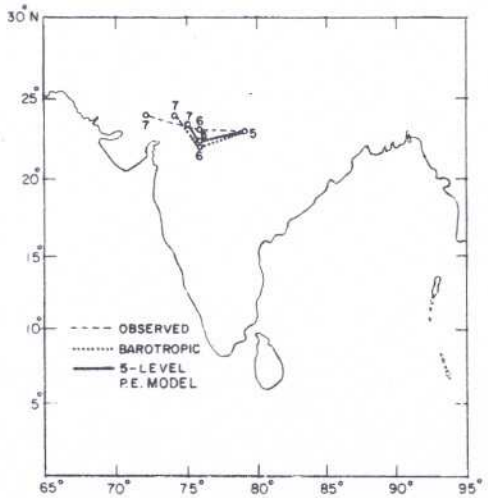

Figure 9. Observed versus predicted tracks in two different numerical prediction experiments.

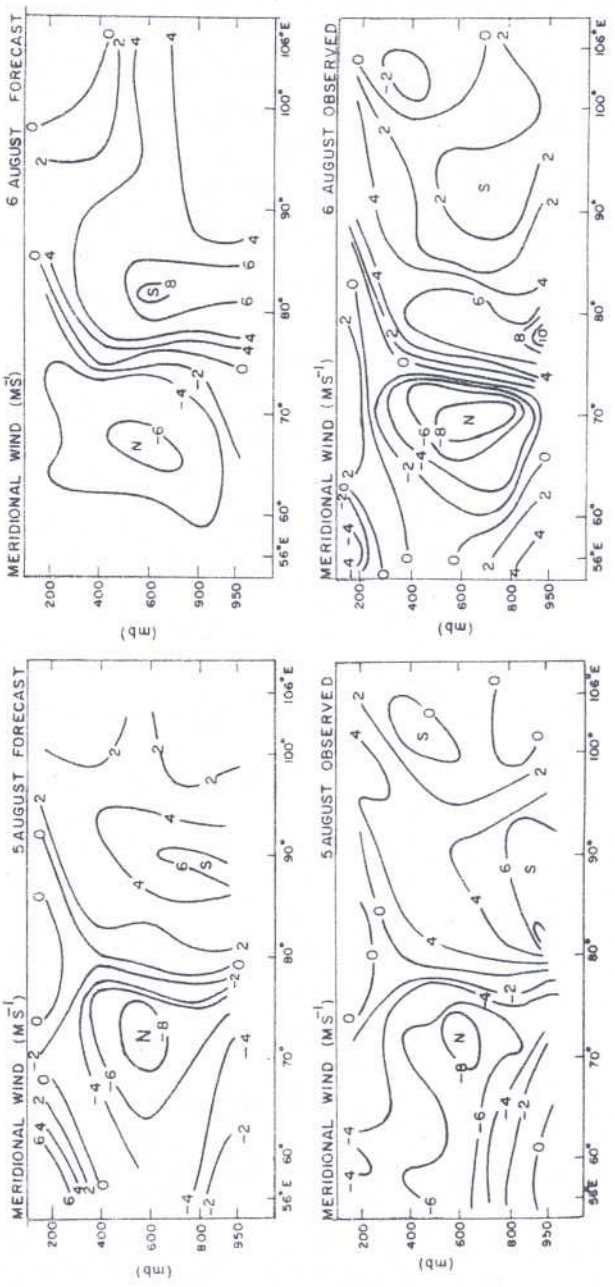

Figure 10. Observed versus predicted field of meridional wind v (m sec^{-1}) at 22°N for 0 and 24 hr. The cross-sections are on a zonal vertical plane.

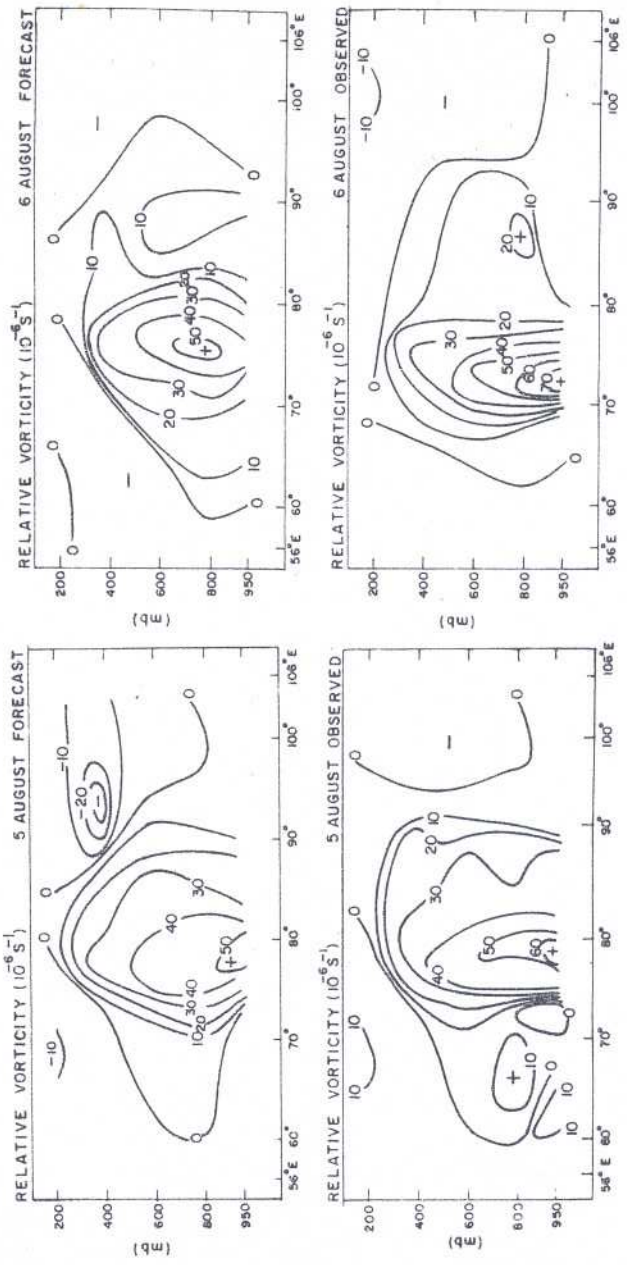

Figure 11. Observed versus predicted field of relative vorticity (sec^{-1}) at 22°N for 0 and 24 hr.

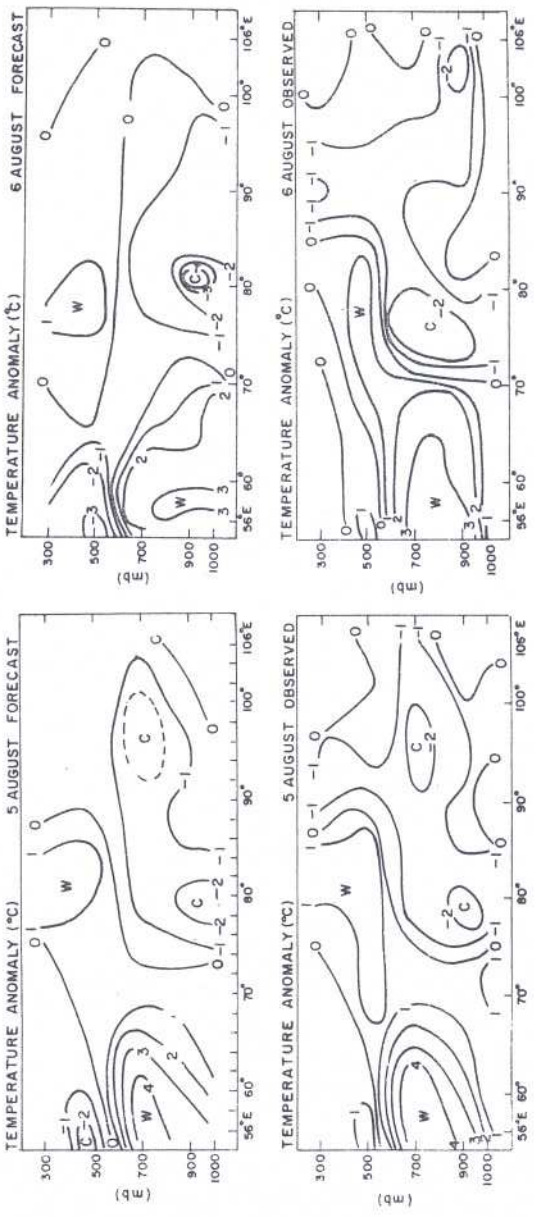

Figure 12. Observed versus predicted field of temperature anomaly (θ_C) at 22°N for 0 and 24 hr.

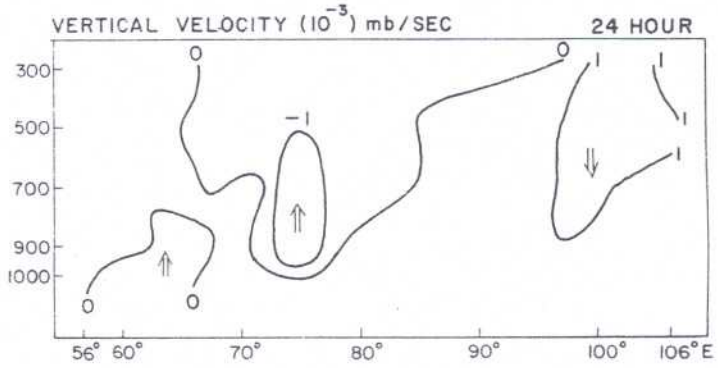

Figure 13. Predicted field of vertical velocity (10^{-3} mb sec^{-1}) at 22°N for 24 hr.

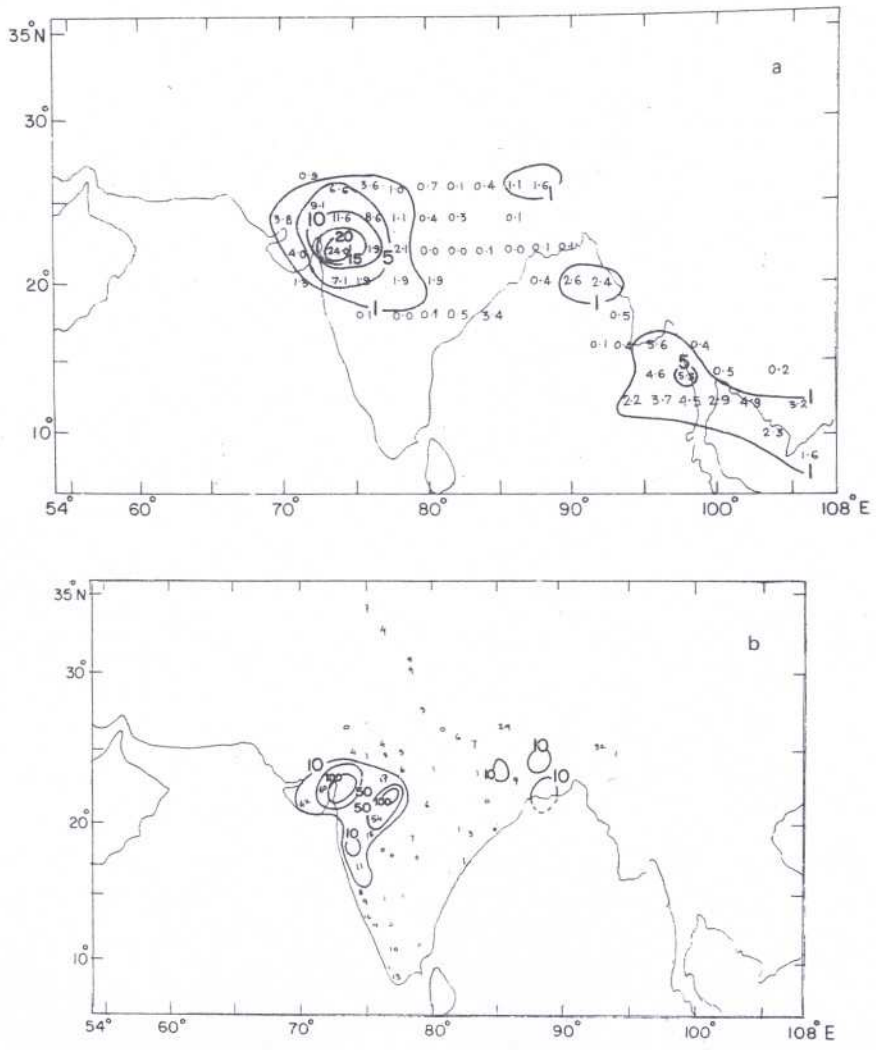

Figure 14. **a.** Predicted and **b.** observed, 24 hr total rainfall amounts (mm).

10. Concluding remarks

The model has produced reasonably good forecast upto 24 hours in respect of the circulation patterns, movement of the cyclonic system, cold core in the lower troposphere and warm core above the surface storm and the precipitation region, and beyond that damped significantly. The intensity of wind and vertical velocity are generally found weaker than the actual, particularly over the cyclonic circulation. The rainfall rates are very much underestimated by the model.

Although the model has produced a reasonably good forecast, it is necessary to point out its deficiency. The model suffers severely from the artificial specification of lateral boundary conditions. The tropical quasi-stationary long waves are a major source of energy for short-waves and the rate of energy transfer from longer waves to synoptic and subsynoptic scale waves is found to be quite large even in the time scale of a few days. For a realistic forecast of the synoptic scale of motion, the interaction of shorter waves with longer waves in model atmosphere should be taken into consideration. This could be accomplished by using a high resolution global model with sophisticated scheme of physical processes. Alternately, the boundary data of the regional model could be provided by the solution of a global model in which the regional model is nested. A third alternative could be to extend the domain of regional model in the east-west and north-south directions to ensure the interaction of different scales. In the present experiment, none of the above could be accomplished mainly due to limited computing facility. Another shortcoming of the model which is considered important is the oscillation of the divergence field during integration. After a few sensitivity experiments, it was noted that the present dynamic initialization which was carried out on limited domain is not capable of suppressing the inertial oscillation completely. This is a severe drawback of the model which is again closely linked with the lateral boundaries. As pointed out in §9.3 the rainfall rates are underestimated by the model. This could be due to unrealistic moisture analysis particularly in the lower troposphere, lack of proper resolution in the planetary boundary layer, weak vertical velocity and to some extent, underestimation of convective rainfall by the scheme of parametrization of cumulus convection in the region where convective rains are predominant. The weak vertical velocity and slow westward propagation of the cyclonic system are to a large extent due to complete absence of orography from the model. Furthermore, the regional model has coarse resolution in the horizontal and vertical directions and should have one more level in the planetary boundary layer and a horizontal grid size of 100 km. To handle the smooth orography effectively, the model should have the earth's surface with detailed orography as a coordinate surface (Phillips 1957). Some of these problems will be examined in future studies.

Acknowledgements

The author thanks Dr Bh V Ramana Murty and Shri D R Sikka for their keen interest. Part of the work was done by the author as WMO Fellow at Meteorological Research Institute, Tsukuba, Japan. He thanks Dr M Yamasaki and Mr H Ohnishi for their helpful discussions in programming the model physics. Thanks are due to Shri A Bandyopadhyay for assistance.

List of symbols

C_p specific heat of air at constant pressure
F_q sub grid scale diffusion of water vapour
F_T sub grid scale diffusion of heat
F_u horizontal diffusion of u-momentum
F_v horizontai diffusion of v-momentum
f Coriolis parameter
f^* $f-m^2u\dfrac{\partial}{\partial y}\left(\dfrac{1}{m}\right)$
f_0 Coriolis parameter at 22°N
g acceleration due to gravity
H vertical eddy flux of sensible heat
M sum of precipitation and evaporation
m map factor
p pressure
q specific humidity
R gas constant for dry air
T temperature
T_s convective cloud temperature
T_v virtual temperature
t time
u zonal wind speed positive towards east
u_{ob} observed zonal wind speed
v meridional wind speed positive towards north
v_{ob} observed meridional wind speed
W vertical eddy flux of water vapour
x coordinate axis towards east
y coordinate axis towards north
z geopotential height
β Rossby parameter $\left(\equiv\dfrac{\mathrm{d}f}{\mathrm{d}y}\right)$
θ potential temperature
τ eddy stress vector
ϕ geopotential
ψ stream function
ω vertical p-velocity
ω_s vertical p-velocity at the surface
$\dfrac{\mathrm{d}Q}{\mathrm{d}t}$ diabatic heating

References

Asselin R 1972 *Mon. Weather Rev.* **100** 487
Bedi H S, Datta R K and Krichak R L 1976 *Meteorol. Gidrol.* **5** 39 (in Russian)
Das P K and Bedi H S 1978 *Indian J. Meteor. Hydrol. Geophys.* **29** 375
Electronic Computation Centre JMA 1980 Outline of the operational numerical weather prediction at JMA, Tokyo, 21 pp

Kanamitsu M 1975 On numerical prediction over global tropical belt Report 75-1, Department of Meteorology, Florida State University, 97 pp
Kiangi P M R 1977 *Arch. Meteorol. Geophys. Bioklimatol.* **A26** 349
Krishnamurti T N, Kanamitsu M, Godbole R, Chang C B, Carr F and Chow J H 1976 *J. Meteorol. Soc. Jpn* **54** 208
Krishnamurti T N, Molinari J, Pan H L and Wong V 1977 *Pure Appl. Geophys.* **115** 1357
Kuo H L 1965 *J. Atmos. Sci.* **22** 40
Kuo H L 1974 *J. Atmos. Sci.* **31** 1232
Leith C E 1969 *Proc. WMO/IUGG symposium on numerical weather prediction, Tokyo* 1968 (Tokyo: Japan Meteorological Agency) Vol. 1, p. 41
Manabe S, Smagorinsky J and Strickler R F 1965 *Mon. Weather Rev.* **93** 769
Okamura Y 1975 *J. Meteorol. Soc. Jpn* **53** 175
Phillips N A 1957 *J. Meteorol.* **14** 184
Singh S S 1977 *Some aspects of prognostic and diagnostic studies of Indian summer monsoon.* Ph.D. thesis, Banaras Hindu University, Varanasi, India, 32–74
Singh S S 1983 A limited area five level primitive equation model, Scientific Report R-038, Indian Institute of Tropical Meteorology, Pune
Singh S S and Saha K R 1976 *Proc. of IITM Symp. on Tropical Monsoons, Pune, India* 1976 p. 43
Singh S S, Kulkarni A A and Sikka D R 1980 *Mon. Weather Rev.* **108** 1315
Temperton C 1976 *Q. J. R. Meteorol. Soc.* **102** 297
Winninghoff F J 1973 *Mon. Weather Rev.* **101** 79